
DNAEdit: Direct Noise Alignment for Text-Guided Rectified Flow Editing

Chenxi Xie^{1,2,*}, Minghan Li^{3,*}, Shuai Li¹, Yuhui Wu^{1,2}, Qiaosi Yi^{1,2}, Lei Zhang^{1,2,†}

¹The Hong Kong Polytechnic University, ²OPPO Research Institute,

³Harvard AI and Robotics Lab, Harvard University

chenxi.xi@connect.polyu.hk mili4@meei.harvard.edu cslzhang@comp.polyu.edu.hk

*Equal contribution †Corresponding author

Project Page: <https://xiechenxi99.github.io/DNAEdit/>

Abstract

Leveraging the powerful generation capability of large-scale pretrained text-to-image models, training-free methods have demonstrated impressive image editing results. Conventional diffusion-based methods, as well as recent rectified flow (RF)-based methods, typically reverse synthesis trajectories by gradually adding noise to clean images, during which the noisy latent at the current timestep is used to approximate that at the next timesteps, introducing accumulated drift and degrading reconstruction accuracy. Considering the fact that in RF the noisy latent is estimated through direct interpolation between Gaussian noises and clean images at each timestep, we propose Direct Noise Alignment (DNA), which directly refines the desired Gaussian noise in the noise domain, significantly reducing the error accumulation in previous methods. Specifically, DNA estimates the velocity field of the interpolated noised latent at each timestep and adjusts the Gaussian noise by computing the difference between the predicted and expected velocity field. We validate the effectiveness of DNA and reveal its relationship with existing RF-based inversion methods. Additionally, we introduce a Mobile Velocity Guidance (MVG) to control the target prompt-guided generation process, balancing image background preservation and target object editability. DNA and MVG collectively constitute our proposed method, namely DNAEdit. Finally, we introduce DNA-Bench, a long-prompt benchmark, to evaluate the performance of advanced image editing models. Experimental results demonstrate that our DNAEdit achieves superior performance to state-of-the-art text-guided editing methods. Codes and benchmark will be available at <https://xiechenxi99.github.io/DNAEdit/>.

1 Introduction

Recent advances in text-to-image (T2I) generation have been driven by Rectified Flow (RF)-based models [13, 12], which significantly reduce sampling timesteps, enabling faster generation. Leveraging large-scale T2I models such as SD3 [3] and FLUX [8], training-free text-guided image editing methods [18, 25, 7, 33] can achieve high-quality editing results with fewer sampling steps. Existing RF-based editing methods [18, 7, 2, 25, 28, 30, 33] typically follow earlier Diffusion Model (DM)-based editing approaches [16, 6, 15], first reversing the generative trajectory by gradually adding noise to the clean image, obtaining an inverted noise and then re-denosing it under new conditions to generate the edited image, as shown by the black path in Fig. 1 (a). The inverted noise is critical for the preservation of fidelity, as it retains the structural information of the reference image, ensuring consistency between the edited and the reference images. However, this inversion process introduces accumulated drifts that significantly degrade reconstruction accuracy and editing fidelity. These drifts

This work is supported by the PolyU-OPPO Joint Innovative Research Center.

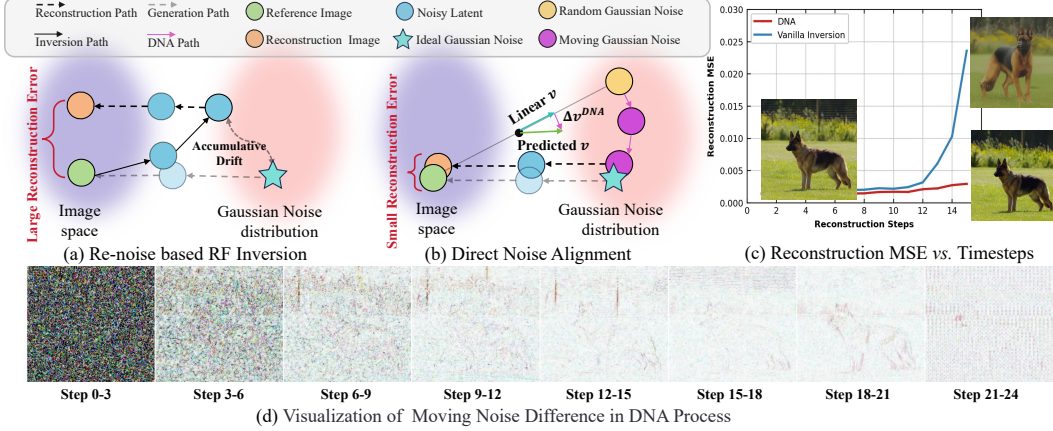


Figure 1: Illustration of (a) existing re-noise based RF inversion methods and (b) our DNA. The ideal Gaussian noise refers to the noise that can exactly reproduce the reference image. (c) The curves of reconstruction MSE vs. timesteps for DNA and re-noise based RF inversion. (d) Visualization of the difference in Gaussian noise between steps.

arise because the noise latent at the current timestep is unavailable and it has to be approximated using the noise latents from the previous timesteps. The approximated latent is then used to estimate the velocity field for inversion, resulting in shifted velocity fields. As the process continues, the drifts accumulate, leading to significant distortions in the final noise.

Existing RF-based methods [18, 2, 14, 25, 28] aim to reduce the drift to improve editing fidelity. For example, RF-inversion [18] employs two conditional velocity fields: one for inversion (conditioned on Gaussian noise) and one for editing (conditioned on the source image). However, its global application of guidance ignores region specificity, often degrading edit quality. Subsequent methods [2, 25, 14], such as RF-solver [25], refine the discretization process using higher-order ordinary differential equation (ODE) solvers, often combined with attention injection during editing to enhance fidelity. More recently, FTEdit [28] reduces errors by performing iterative average at each inversion timestep, increasing the number of sampling steps. While these approaches reduce errors through finer discretization of the reverse ODE process, they incur additional Neural Function Evaluations (NFEs), decreasing the efficiency. Despite offering slight improvements over RF inversion, these methods remain inefficient and struggle to mitigate the accumulation and amplification of drift.

Actually, existing editing methods overlook the unique properties of RF. Unlike DM, RF models the generation process as a straight trajectory between noise and image, allowing noise latent to be derived via linear interpolation at each timestep. Keeping this in mind, let us revisit the editing process. Note that inversion aims to estimate a noise sample that corresponds to the reference image, enabling an accurate reconstruction of it during sampling. In RF, a better noise sample means a more direct path between the noise and the reference image. Based on this, an intuitive question is: *can we directly refine the desired noise sample in the Gaussian noise domain, rather than gradually transforming the image into noise?* To answer this question, we propose a novel method in this work, called **Direct Noise Alignment Editing (DNAEdit)**. Unlike gradually transforming an image back to Gaussian noise, *DNAEdit directly refines the randomly initialized noise in the Gaussian noise domain, gradually aligning it with a better target noise sample*, as shown in Fig. 1 (b).

To achieve Direct Noise Alignment (DNA), we start from a Gaussian noise sample and iteratively interpolate between it and the clean reference image at each timestep. As shown in Fig. 1 (b), the predicted velocity field often deviates from the expected one derived from linear interpolation. DNA, thus, corrects it by feeding the deviation back into the noise, refining the trajectory. We visualize the changes during the DNA process in Fig. 1 (d). These changes contain the structure of the original image, indicating that the original content is gradually infused into the initial random noise, resulting structured noise. This process produces straighter paths and reduces the accumulated error by avoiding dependence on previous random noise and latents. Finally, the noise converges to a sample that is well aligned with the reference image, as verified by the reconstruction MSE in Fig. 1(c). We also provide a theoretical analysis showing that DNA shares the same principle with RF-based methods in the **Appendix**.

To better balance editability and fidelity, we introduce a Mobile Velocity Guidance (MVG) to guide denoising by computing the difference between source- and target-conditioned velocity fields in the image domain, which yields a smooth transition from source to target images. In addition, existing benchmarks [6, 11, 31, 17] focus on short prompts, limiting semantic richness. To address this, we introduce **DNA-Bench**, a long-prompt benchmark to evaluate RF editing under detailed textual guidance. Experiments on PIE-Bench and DNA-Bench show that our DNAEdit method strikes a better balance between fidelity and editability, demonstrating the best performance.

2 Related Work

Inversion for Image Editing. Inversion seeks to transform an image into a corresponding Gaussian noise. A successful inversion generates an initial noise vector that can accurately recreate the reference image, which is essential for further editing. According to DDIM [19], the initial noise can be gradually obtained by iteratively adding predicted noise, but the approximation error can accumulate over timesteps. Various strategies have been developed to address this issue. Null-text inversion [16] optimizes null text embeddings at each inversion step, but it is inefficient. Negative-prompt-inversion improves efficiency by replacing null texts with negative prompts. Unlike DMs, RF has a notably straighter generation path. However, current RF inversion methods still adhere to DM principles, reversing the ODE to gradually add noise. RF inversion [18] aims to tackle this issue by optimizing the reverse ODE process using dynamic optimal control through a linear quadratic regulator to balance editability and fidelity. RF-solver [25] and FireFlow [2] use higher-order solvers to better approximate the reverse ODE and reduce errors at each step. FTEdit [28] employs a fixed-point iteration strategy, refining the added noise and averaging it to suppress approximation errors. Although these approaches can reduce reconstruction error to some extent, they all follow the iterative re-noising paradigm, making error accumulation inevitable. In contrast, our proposed DNA framework directly aligns the noisy latent with the ideal noise derived from model priors within the noise space, significantly reducing the error accumulation.

Rectified Flow-based Editing. Compared to DM-based editing methods [1, 23, 4, 5], RF-based editing methods are not fully explored. Unlike most DM models that use the U-Net architecture, RF models [8, 3] primarily use the MM-DiT architecture, which makes strategies relying on U-Net’s cross-attention map unsuitable for RF-based editing methods. Some approaches [2, 25] adapt the attention injection scheme to maintain fidelity during editing. Other methods [28] focus on the exchange of text-image information in MM-DiT, manipulating features through AdaLN to control the editing process. While these methods have achieved certain success, they often require additional adaptations for different RF models, limiting their applicability. Some model-agnostic methods have also been developed. FlowEdit [7] uses an inversion-free approach by calculating the difference between the source and the target velocity fields, enabling direct image editing in the image space. However, this method relies on editing the velocity difference of the reference image and restricts the range of editable space, making it difficult to perform global editing tasks (*e.g.*, changing style). Our DNAEdit employs two model-agnostic processes: DNA and MVG. DNA minimizes cumulative error and obtain a better initial Gaussian noise aligned with the source text. MVG guides the editing process to preserve background fidelity while minimizing compromise on editability.

3 Direct Noise Alignment Editing (DNAEdit)

3.1 Approximation Errors in RF Inversion

Preliminary. Rectified Flow (RF) [13, 12] models the transition between two observed distributions π_0 and π_1 using an ordinary differential model (ODE):

$$dZ_t = v_\theta(Z_t)dt, \quad Z_0 \sim \pi_0, \quad Z_1 \sim \pi_1, \quad t \in [0, 1], \quad (1)$$

where $v_\theta(\cdot)$ is the learnable velocity field parameterized by θ . To encourage a near-linear trajectory of the transition, RF employs the following objective to train v_θ :

$$\min_{\theta} \int_0^1 \mathbb{E}[\|(Z_1 - Z_0) - v_\theta(Z_t)\|^2]dt, \quad Z_t = tZ_1 + (1-t)Z_0, \quad (2)$$

where Z_t denotes the linear interpolation between $Z_0 \sim \pi_0$ and $Z_1 \sim \pi_1$.

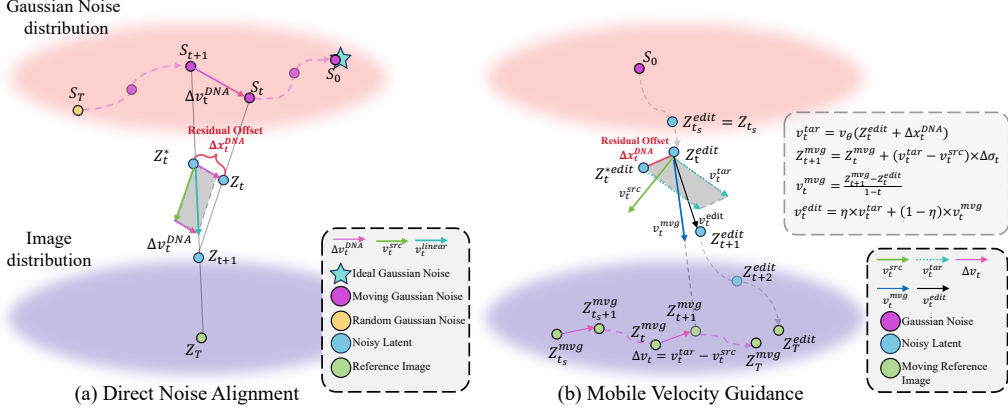


Figure 2: Illustration of (a) DNA and (b) MVG, which collectively build our DNAEdit algorithm.

Approximation Errors in Inversion. The denoising process maps the standard Gaussian distribution ($\pi_0 = \mathcal{N}(0, 1)$) to the image distribution π_1 , while its reverse maps π_1 back to π_0 . To solve the ODE in Eq. (1), the time interval $[0, 1]$ is discretized into T steps, denoted as $\{\sigma_0, \dots, \sigma_T\}$. The Euler solver is used to approximate the solution, with the forward and reverse steps given by:

$$\text{Fwd} : Z_{t+1} = Z_t + v_\theta(Z_t)(\sigma_{t+1} - \sigma_t), \quad \text{Inv} : Z_t = Z_{t+1} - v_\theta(Z_t)(\sigma_{t+1} - \sigma_t), \quad (3)$$

where the timestep index increases from 0 to T in the forward process and decreases from T to 0 in the reverse process. It is evident that in the reverse process, at each step only the noisy latent Z_{t+1} is available, while Z_t , the desired output, is unknown. Consequently, the velocity field $v_\theta(Z_t)$ in Eq. (3) cannot be directly evaluated, making the exact inversion intractable.

Considering that the differences between the noisy latents of adjacent timesteps are relatively small, existing RF inversion methods [2, 25, 18, 28] approximate the velocity field at timestep t by evaluating it at timestep $t + 1$, leading to the following inversion formula:

$$\text{Inv approx} : v_\theta(Z_t) \approx v_\theta(Z_{t+1}), \quad Z_t \approx Z_{t+1} - v_\theta(Z_{t+1})(\sigma_{t+1} - \sigma_t). \quad (4)$$

However, due to the sequential nature of the inversion process, approximation errors at each step will accumulate over time, resulting in a final latent that can deviate significantly from the expected Gaussian noise (see Fig. 1 (a)). Furthermore, the noise sample obtained through this approximated inversion is not guaranteed to follow the standard Gaussian distribution, mismatching with the model assumption. As a result, the reconstructed or edited image (see Fig. 1 (c)) may be distorted or invalid.

3.2 Direct Noise Alignment (DNA)

Our DNAEdit method consists of two key components: DNA and MVG (see Section 3.3). DNA is used to obtain a structured noise sample, enhancing the fidelity of the editing process. The resulting noise is then re-denoised under the guidance of MVG to generate the final image. From the analysis in Section 3.1, we see that the primary source of error comes from the use of the noisy latent Z_{t+1} to replace Z_t to compute the velocity field: $v_\theta(Z_t) \approx v_\theta(Z_{t+1})$. Since the noise levels of Z_t and Z_{t+1} are different, this approximation introduces inconsistencies with the model prior.

Using RF, fortunately, the latent variables Z_t can be constructed via linear interpolation between the clean image and Gaussian noise. One can sample a noise $S \sim \mathcal{N}(0, 1)$ and interpolate it with the image. However, since S is randomly sampled, the resulting path may lead to reconstruction errors under text guidance. According to Eq. (2), there exists an optimal noise such that the RF-driven trajectory forms a nearly linear path to the reference image. Motivated by this, we propose *directly shifting the random noise toward the target noise in the Gaussian space over timesteps*: $S_T \sim \mathcal{N}(0, 1) \rightarrow S_{T-1} \rightarrow \dots \rightarrow S_0$.

To achieve this goal, we need to devise an effective algorithm to optimize random Gaussian noise S_T . This can be done by aligning the velocity v_t^{src} predicted by the RF model with the expected velocity v_t^{linear} along the linear path from Gaussian noise to image latent. Specifically, at timestep t ,

Algorithm 1 Direct Noise Alignment (DNA)

Input: Number of optimization steps T , Source image Z_T , Source text ψ^{src} , Timesteps $\{\sigma_t\}_{t=T}^0$, RF model v_θ with parameters θ , Randomly sampled start noise $S_T \sim \mathcal{N}(0, 1)$.

Output: Noisy latents $\{Z_t\}_{t=T-1}^0$ and residual offset $\{\Delta x_t^{DNA}\}_{t=T-1}^0$, Terminal noise sample S_0

for $t = T - 1, \dots, 1, 0$ **do**

$$Z_t^* \leftarrow Z_{t+1} \times \frac{\sigma_t}{\sigma_{t+1}} + S_{t+1} \times (1 - \frac{\sigma_t}{\sigma_{t+1}}) \quad \triangleright \text{Interpolate to get noisy latent } Z_t^*$$

$$v_t^{\text{linear}} = (S_{t+1} - Z_{t+1})/\sigma_{t+1} \quad \triangleright \text{Calculate the expected velocity on the linear path}$$

$$v_t^{src} = v_\theta(Z_t^*, \psi^{src}) \quad \triangleright \text{Calculate the predicted velocity by SD3 or FLUX}$$

$$\Delta v_t^{DNA} = v_t^{\text{linear}} - v_t^{src}$$

$$S_t \leftarrow S_{t+1} + \Delta v_t^{DNA} \times \sigma_{t+1} \quad \triangleright \text{Move Gaussian noise from } S_{t+1} \text{ to } S_t$$

$$Z_t \leftarrow Z_t^* + \Delta v_t^{DNA} \times (\sigma_{t+1} - \sigma_t) \quad \triangleright \text{Move interpolated latent from } Z_t^* \text{ to } Z_t$$

$$\Delta x_t^{DNA} = Z_t^* - Z^* \quad \triangleright \text{Compute the residual offset}$$

end for

return $S_0, \{Z_t\}_{t=T-1}^0$ and $\{\Delta x_t^{DNA}\}_{t=T-1}^0$

we construct the linear path from noise S_{t+1} to latent Z_{t+1} and obtain latent Z_t^* by interpolation:

$$Z_t^* = \frac{\sigma_t}{\sigma_{t+1}} \times Z_{t+1} + (1 - \frac{\sigma_t}{\sigma_{t+1}}) \times S_{t+1}. \quad (5)$$

The estimated noisy latent Z_t^* is obtained via direct interpolation, eliminating the need to approximate it using Eq. (4). We then compute the velocity field Z_t^* using the RF model as $v_t^{src} = v_\theta(Z_t^*, \psi^{src})$, and define the expected velocity along the linear path as $v_t^{\text{linear}} = (S_{t+1} - Z_{t+1})/\sigma_{t+1}$. However, as shown in Fig. 2(a), a discrepancy arises between v_t^{linear} and v_t^{src} due to the offset between the actual noise S_{t+1} and the noise S_t derived by the predicted velocity. We denote this mismatch as the velocity gap Δv_t^{DNA} , and correct it by shifting the noise from S_{t+1} to S_t :

$$\Delta v_t^{DNA} = v_t^{\text{linear}} - v_t^{src}, \quad S_t = S_{t+1} + \Delta v_t^{DNA} \times \sigma_{t+1}. \quad (6)$$

As the noise moves to S_t , the interpolated noisy latent Z_t^* in Eq. (5) can be refined to a better estimate $Z_t = \frac{\sigma_t}{\sigma_{t+1}} \times Z_{t+1} + (1 - \frac{\sigma_t}{\sigma_{t+1}}) \times S_t$. It can be easily derived that the updated linear velocity $v_t^{\text{linear}} = (S_t - Z_{t+1})/\sigma_{t+1}$ matches the predicted velocity $v_\theta(Z_t^*, \psi^{src})$. The difference between the updated latent Z_t and the initial estimate Z_t^* can be expressed as:

$$Z_t - Z_t^* = \frac{\sigma_{t+1} - \sigma_t}{\sigma_{t+1}} \times (S_t - S_{t+1}). \quad (7)$$

By substituting Eq. (6) into Eq. (7), we can derive that $Z_t = Z_t^* + \Delta v_t^{DNA} \times (\sigma_{t+1} - \sigma_t)$. Eq. (7) implies that although the random Gaussian noise S_T may initially deviate from the ideal Gaussian noise, the difference will become much smaller for interpolated latent Z_t due to the small scaling coefficient $(\sigma_{t+1} - \sigma_t)/\sigma_{t+1}$, where $\sigma_{t+1} : 1 \rightarrow 0$. Therefore, it can be deduced that $v_\theta(Z_t, \psi^{src}) \approx v_\theta(Z_t^*, \psi^{src})$. Starting from Z_t , the predicted velocity field can lead to Z_{t+1} with a small error. Eq. (7) suggests aligning from large to small timesteps to avoid early errors, so we iteratively adjust noise from σ_T to σ_0 . We also show that the residual offset $\Delta x_t^{DNA} = Z_t^* - Z_t$ allows exact reconstruction. Adding it back to Z_t , we recover Z_t^* and compute $v_\theta(Z_t^*, \psi^{src})$ for precise updates from Z_t to Z_{t+1} . The algorithm is presented in Algorithm 1, and a theoretical analysis between DNA and existing RF-based methods is provided in the **Appendix**.

3.3 Mobile Velocity Guidance (MVG)

Although DNA can estimate a noise sample with small reconstruction error, directly using target texts to guide image generation may destroy the original structure of the reference image. Inspired by [18], we can control the fidelity of the edited image by integrating the velocity field pointed to the reference image. However, if the velocity field is introduced improperly, it can interfere with the denoising process, resulting in *an undesired overlay of the reference and target images* and degrading editability. To address this, we introduce *Mobile Velocity Guidance* (MVG), as illustrated in Fig. 2(b), which adaptively guides the editing process to balance fidelity and editability.

The denoising process starts from a noise sample and gradually moves it to the target image, forming a trajectory from Gaussian noise to the target, called Z_t^{edit} . Specifically, at timestep t , we first

Algorithm 2 Mobile Velocity Guidance (MVG)

Input: Source image Z_T , Timesteps $\{\sigma_t\}_{t=0}^T$, RF $v_\theta(\cdot)$, Noisy latents $\{Z_t\}_{t=T-1}^0$, Residual gaps $\{\Delta x_t^{\text{DNA}}\}_{t=T-1}^0$, Start Step t_s , Target text ψ^{tgt}

Output: Edited Image Z_T^{edit}

Init: $Z_{t_s}^{\text{edit}} = Z_{t_s}$, $Z_{t_s}^{\text{mvg}} = Z_T$

for $t = t_s, t_s + 1, \dots, T - 1$ **do**

$v_t^{tgt} = v_\theta(Z_t^{\text{edit}}, \psi^{tgt})$, $Z_t^{*\text{edit}} \leftarrow Z_t^{\text{edit}} + \Delta x_t^{\text{DNA}}$ ▷ Involve residual gap to get target velocity

$v_t^{src} = v_\theta(Z_t^*, \psi^{src}) = \frac{Z_{t+1} - Z_t}{\sigma_{t+1} - \sigma_t}$, $\Delta v_t = v_t^{tgt} - v_t^{src}$ ▷ Reuse source velocity from DNA latents

$Z_{t+1}^{\text{mvg}} \leftarrow Z_t^{\text{mvg}} + \Delta v_t \times (\sigma_{t+1} - \sigma_t)$ ▷ Move the mobile latent toward the target image

$v_t^{\text{mvg}} = (Z_t^{\text{edit}} - Z_{t+1}^{\text{mvg}}) / (1 - \sigma_t)$ ▷ Calculate the mobile velocity guidance

$v_t^{\text{edit}} = \eta \times v_t^{tgt} + (1 - \eta) \times v_t^{\text{mvg}}$ ▷ Calculate the synthesized denoising velocity

$Z_{t+1}^{\text{edit}} \leftarrow Z_t^{\text{edit}} + v_t^{\text{edit}} \times (\sigma_{t+1} - \sigma_t)$ ▷ Perform denoising step

end for

return Z_T^{edit}

incorporate Δx_t^{DNA} to shift Z_t^{edit} to $Z_t^{*\text{edit}}$, enabling the exact computation of target velocity v_t^{tgt} :

$$Z_t^{*\text{edit}} = Z_t^{\text{edit}} + \Delta x_t^{\text{DNA}}, \quad v_t^{tgt} = v_\theta(Z_t^{*\text{edit}}, \psi^{tgt}). \quad (8)$$

This step is crucial. According to Eq. (7), the residual $\Delta x_t^{\text{DNA}} = Z_t^* - Z_t$ is equivalent to the weighted difference between two Gaussian noise samples and therefore free from image content. Essentially, this operation ensures that the regions intended to be preserved in $Z_t^{*\text{edit}}$ are perfectly aligned with the noisy latent in the reverse process, *i.e.*, Z_t^* in Eq. (5). As a result, the computed target and source velocities (v_t^{tgt} and v_t^{src}) become near-identical in those preserved regions, which not only improves reconstruction accuracy but also significantly enhances editing fidelity. Our ablation study in **Appendix** further supports this finding.

In addition, there exists another trajectory that transitions from the source image to the target image purely within the image space, denoted as Z_t^{mvg} . Before using v_t^{tgt} to update the noisy latent Z_t^{edit} conditioned on the target text, we first apply the velocity difference between the source and target to shift Z_t^{mvg} from the reference image toward the target image. This velocity difference and the corresponding mobile latent modification are defined as:

$$\Delta v_t = v_t^{tgt} - v_t^{src}, \quad Z_{t+1}^{\text{mvg}} = Z_t^{\text{mvg}} + \Delta v_t \times (\sigma_{t+1} - \sigma_t). \quad (9)$$

Here, we use the saved latents in DNA to calculate the velocity v_t^{src} , which not only reduces the number of function evaluations (NFEs) but also accurately captures the velocity field associated with the reconstruction of the reference image. The velocity difference Δv_t is then applied to the mobile reference image Z_t^{mvg} , modifying specific regions to reflect the differences induced at timestep t under the source and target text conditions. Using the updated latent Z_{t+1}^{mvg} , we obtain the final denoising velocity by blending the velocity fully conditioned on the target text v_t^{tgt} with the MVG v_t^{mvg} using a weighting coefficient η as :

$$v_t^{\text{mvg}} = (Z_t^{\text{edit}} - Z_{t+1}^{\text{mvg}}) / (1 - \sigma_t), \quad v_t^{\text{edit}} = \eta \times v_t^{tgt} + (1 - \eta) \times v_t^{\text{mvg}}, \quad (10)$$

where $\eta \in [0, 1]$ controls the trade-off between fidelity and editability.

Finally, we apply the synthesized velocity to perform the denoising by $Z_{t+1}^{\text{edit}} = Z_t^{\text{edit}} + v_t^{\text{edit}}(\sigma_{t+1} - \sigma_t)$. This process is applied across all timesteps, as shown in Fig. 2(b). To avoid excessive changes during editing, we skip the initial step and select Z_{t_s} as the starting point for editing. The complete algorithm of MVG is summarized in Algorithm 2. Using a fixed reference image for guidance, as in [18], we maintain the denoising direction close to the reconstruction of the source image during the early editing stages, thereby enhancing the fidelity. However, in later stages, as the image content undergoes substantial changes, relying on the original reference image can severely hinder editability. In contrast, our proposed MVG v_t^{mvg} mitigates this issue by employing a moving reference for guidance, effectively balancing fidelity and editability throughout the editing process.

Table 2: Quantitative comparison on PIE-Bench. Red, blue, yellow represents top 3 performers.

Method	Model	Structure	Background Preservation					CLIP Similarity		Rank
		Distance ↓	PSNR ↑	LPIPS ↓	MSE ↓	SSIM ↑	Whole ↑	Edited ↑	Avg. ↓	
PnP[23]	SD1.5	27.35	22.31	112.76	82.95	79.25	25.41	22.52	9.17	
MasaCtrl[1]	SD1.4	27.12	22.19	105.44	86.37	79.91	24.03	21.15	10.42	
DI+PnP[6]	SD1.5	23.35	22.46	105.51	79.94	79.88	25.49	22.64	6.83	
DI+MasaCtrl[6]	SD1.4	23.58	22.68	87.41	80.63	81.51	24.39	21.41	8.75	
InfEdit[29]	LCM	19.31	27.31	56.32	47.80	85.30	24.90	22.14	5.67	
InsP2P[4]	InsP2P	58.13	20.80	159.23	221.3	76.47	23.61	21.68	13.42	
RF-Inv[18]	FLUX	42.29	20.20	179.54	139.2	69.91	24.57	22.20	12.42	
RFEdit[25]	FLUX	21.79	24.83	113.15	52.46	83.38	25.57	22.26	6.42	
FireFlow[2]	FLUX	29.03	23.33	133.40	70.83	81.22	26.19	22.99	7.42	
FlowEdit[7]	FLUX	27.82	21.96	112.19	94.99	83.08	25.25	22.58	9.50	
FlowEdit[7]	SD3	27.12	22.22	104.12	85.96	93.22	26.53	23.57	5.58	
FTEdit[28]*	SD3.5	18.17	26.62	80.55	40.24	91.50	25.74	22.27	3.50	
DNAEdit (Ours)	FLUX	18.87	24.99	95.06	50.45	85.71	25.79	22.87	3.42	
DNAEdit (Ours)	SD3.5	14.19	26.66	74.57	32.76	88.63	25.63	22.71	2.50	

4 Experiments

4.1 Experimental Settings

DNA-Bench. Text-guided editing has been extensively studied, and evaluation benchmarks [6, 11, 17] have been proposed to evaluate and compare the different editing methods. However, most of these benchmarks are developed in conjunction with diffusion-based models. Due to the limitations of text encoders and pre-trained models, diffusion models struggle to accurately understand long text inputs. As a result, existing benchmarks typically feature short descriptions. For example, PIE-Bench [6] has an average prompt length of **9.46** words. In contrast, RF-based models have shown significant improvements in understanding long text input, but the short descriptions in existing benchmarks cannot fully evaluate the editing capabilities of RF-based models.

To bridge this gap, we propose an extended version of PIE-Bench, called DNA-bench, which is tailored for long-text prompts. To construct DNA-Bench, we design target-aware prompts and leverage the powerful multimodal large language model GPT-4o [22] to generate detailed descriptions of the source images as source prompts. In addition, we modify and extend the original target prompts to align with the editing tasks. The average prompt length in DNA-bench is **33.17** words. More details of the construction process and example prompts of DNA-Bench can be found in the **Appendix**.

Implementation and Compared Methods. Two versions of DNAEdit are provided, which are based on FLUX-dev [9] and SD3.5-medium [20], respectively. In both versions, the MVG coefficient η is fixed at 0.8. Detailed hyper-parameter settings can be found in the **Appendix**. We compare DNAEdit with representative DM-based methods [1, 23, 29] and latest RF-based editing methods [18, 25, 2, 7, 28] using their official implementations and default settings in a shared environment, except FTEdit, where we use provided results.

Evaluation and Metrics. We first conduct **reconstruction** and **text-guided editing** experiments on the PIE-bench [6]. The PIE-bench consists of 700 natural and artificial images to evaluate editing methods across 9 distinct dimensions. It provides the source and target prompts for each image, along with the editing area masks to assess background preservation and local editing ability. We then conduct experiments on our proposed DNA-bench. To evaluate the reconstruction and preservation performance of non-edited areas, we adopt the commonly used image quality metrics, including

Table 1: Quantitative results on reconstruction.

Method	NFE↓	MSE↓	LPIPS↓	SSIM↑
Vallina Inversion	60	0.028	0.342	0.601
RF-Inversion [18]	56	0.023	0.279	0.526
RFEdit [25]	60	0.022	0.244	0.677
FireFlow [2]	57	0.015	0.200	0.726
DNA	56	0.010	0.110	0.830

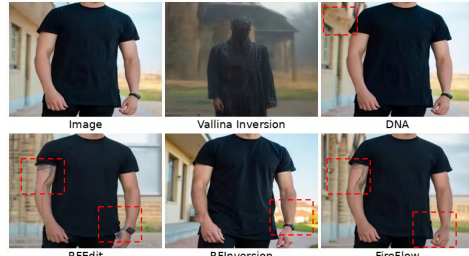


Figure 3: Qualitative comparison on reconstruction.

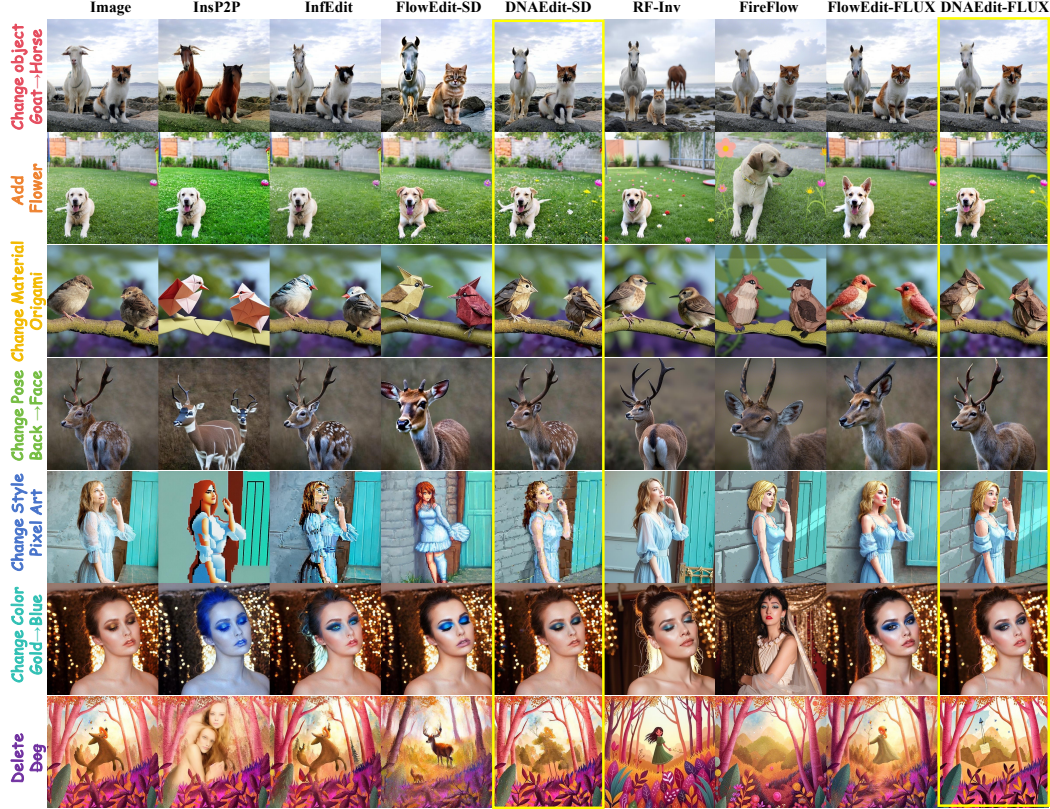


Figure 4: Qualitative comparison of different text-guided image editing methods.

LPIPS [32], SSIM [26], MSE, PSNR and structure distance [6]. Meanwhile, CLIP similarity [27] is employed to assess the consistency between target prompts and edited results.

4.2 Main Results

Results on Reconstruction. In Fig. 3, we present a qualitative comparison among different RF-based reconstruction methods. We see that our DNA method surpasses other approaches in reconstruction accuracy, with only minor differences from the original image in the area highlighted by red-box. FireFlow and RFEdit both use higher-order ODEs to reduce inversion drift, achieving good overall accuracy. However, noticeable differences appear in areas such as the background and arms. RF-Inversion uses the original image as a reference during reconstruction, leading to over-generation, such as the house in the background, which is not faithful to the original image. Moreover, using the original image as a reference can compromise the editability during editing. The quantitative results are reported in Section 4. Compared to existing inversion-based methods [2, 18, 25], our DNA achieves the lowest reconstruction error under similar NFEs.

Quantitative Comparison on Text-guided Editing. In Table 2, we evaluate editing methods in three dimensions: structure preservation, background preservation, and clip similarity. We present the overall ranking for each method by averaging the rankings in these dimensions in the last column of Table 2. Our approach demonstrates superior overall performance, particularly in terms of structure and background preservation. Specifically, while InfEdit shows better PSNR and LPIPS metrics, its CLIP similarity is significantly lower than other methods. This suggests that its strong background preservation hinders its editing capabilities. FlowEdit-SD3 achieves a higher CLIP score but shows weaker background and structure preservation compared to our method (PSNR 22.22dB vs. 26.66dB), indicating potential over-editing. This is attributed to its use of a large CFG in the generation, which also leads to poorer visual quality, as illustrated in Fig. 4. Lastly, the recently developed FTEdit shows relatively balanced performance. However, our method excels in background and structure preservation, with similar whole CLIP scores (25.63 vs. 25.74). In edited regions, our DNAEdit achieves a notably higher CLIP score, 22.71 vs. 22.27, indicating that our approach better preserves

Table 3: Quantitative Results on DNA-Bench. Red, blue, yellow represents top 3 performers.

Method	Model	Structure	Background Preservation					CLIP Similarity		Rank
		Distance ↓	PSNR ↑	LPIPS ↓	MSE ↓	SSIM ↑	Whole ↑	Edited ↑	Avg. ↓	
RFedit	FLUX	20.18	25.13	104.92	49.46	84.01	28.34	22.99	2.92	
RF-Inversion	FLUX	41.92	20.18	176.40	139.69	69.96	27.98	22.89	6.83	
FlowEdit	SD3	30.93	21.35	118.48	103.52	81.45	28.89	23.58	4.58	
FlowEdit	FLUX	29.06	21.57	116.97	102.50	82.54	28.15	22.86	5.33	
FireFlow	FLUX	26.97	23.57	124.78	68.51	81.82	28.69	23.32	3.83	
DNAEdit	FLUX	18.61	24.89	93.76	50.80	85.80	28.36	22.99	2.41	
DNAEdit	SD3.5	25.67	23.24	112.60	67.32	83.69	28.90	23.66	2.08	

non-edited areas while accurately editing targeted regions. Furthermore, our method is model-agnostic and does not require alterations to the MM-DiT architecture, enhancing its applicability.

Qualitative Comparison on Text-guided Editing. We present visual comparisons of state-of-the-art editing methods in Fig. 4, including object, attribute, color, material, style, and pose editing. It can be found that InfEdit often results in edits without visible changes (see the 2nd, 4th and 7th rows). In contrast, FireFlow frequently exhibits over-editing, as shown in the 2nd, 4th and 6th rows. Although the editing instructions are followed, the original image’s structure is significantly changed. As for FlowEdit, while the SD3 version of it successfully accomplishes most editing tasks without altering much the original image’s structure, it suffers from low visual quality and noticeable over-saturation, as evident in row 1 and row 4. The FLUX version of FlowEdit offers better visual quality, but it has some shortcomings in fidelity and instruction following for some editing tasks. For instance, in row 2, it fails to add a flower, and there is a noticeable change in the dog’s ears. Compared to these methods, our proposed DNAEdit method is versatile across various editing tasks and shows superior visual quality. For example, in row 5, our approach successfully applies a global pixel style while preserving the original image’s character pose and overall structure. Similarly, in row 6, our method effectively changes the makeup color while retaining facial ID and other details, achieving desired results for both edited and non-edited areas. In summary, DNAEdit effectively balances between editability and fidelity, which is consistent with our quantitative results.

Results on DNA-Bench. Table 3 shows the results of RF-based editing methods on DNA-Bench. Our DNAEdit remains the best, achieving high clip scores while preserving the background. This validates that DNAEdit can be used for image editing with short- and long-text inputs without any change. Comparing the results of the same method under long and short prompts, we can see that inversion-based methods achieve better background preservation with long prompts (*e.g.*, FireFlow achieves a PSNR of 23.33dB on PIE-Bench and a PSNR of 23.57dB on DNA-Bench). This is because long texts provide detailed descriptions that align with image contents, allowing more accurate reconstruction. As shown in Fig. 5, short prompts change a cat into a dog but alter the pose, while long prompts keep the original pose, producing consistent results. In addition, long prompts also result in improved clip similarity scored.



Figure 5: Visual comparison between editing results using short and long prompt.

4.3 Ablation on Proposed Modules

Baseline. In Table 4, we present the experimental results of our proposed method with different modules. We begin with Exp. ①, which utilizes velocity fields computed on interpolated latents to reverse ODE process. In Exp. ①, we initiate the inversion process by randomly sampling Gaussian noise, which is then used throughout the inversion process. At each step, the Gaussian noise is interpolated with the latent at timestep t to compute the velocity field for timestep $t - 1$, facilitating the inversion. During the re-denoise phase, we use the velocity field conditioned on target prompt to generate target image. By employing interpolation to construct the latent of timestep $t - 1$, we can mitigate errors caused by approximation. As observed, this setting already achieves relatively good results. However, despite avoiding approximation errors at each step, the use of a fixed Gaussian

Table 4: Ablation study on proposed modules.

Exp.	Component	Structure	Background Preservation				CLIP Similarity	
		Distance ↓	PSNR ↑	LPIPS ↓	MSE ↓	SSIM ↑	Whole ↑	Edited ↑
①	Interpolation	31.90	22.61	147.77	84.60	78.93	25.73	22.47
②	+DNA	32.67	22.18	146.27	89.92	79.73	26.24	23.08
③	+ResOffset	24.93	23.75	120.56	64.81	82.24	26.02	22.79
④	+DNA +ResOffset	33.98	21.97	149.84	95.19	79.32	26.40	23.23
⑤	+DNA+MVG	18.81	24.91	95.44	50.29	85.55	25.78	22.48
⑥	+DNA +ResOffset+MVG	18.87	24.99	95.06	50.45	85.71	25.79	22.87

noise throughout the process can introduce significant errors when approaching pure noise, especially if the initially sampled Gaussian noise deviates much the desired structure noise.

Effectiveness of DNA. In Exp. ②, we introduce DNA, adjusting the initially sampled Gaussian noise during the inversion process. By comparing ① and ②, we can observe that as the structural and background preservation metrics remain nearly unchanged, the Clip Whole and Clip Edited similarity significantly increase, from 25.73 and 22.47 to 26.24 and 23.08, respectively. This improvement is attributed to the DNA process, where the noise is continuously moved by the difference between the linear velocity and the velocity conditioned on the source prompt. This movement injects the original image structure and gradually aligns the random noise with the structured noise corresponding to source prompt, enabling the generated results to better match the target prompt during editing.

Effectiveness of ResOffset. Comparing Exp. ① and ③, we see that the introduction of ResOffset during the re-denoising process significantly improves the metrics for image structure and background preservation. For instance, the Structure Distance improves from 31.90 to 24.93, and the PSNR increases from 22.61 dB to 23.75 dB. By incorporating the latent calculated with ResOffset, we shift Z_t^{edit} to Z_t^{*edit} , enhancing the consistency between the intended preserved regions in the noisy latent Z_t^* during the DNA process and those Z_t^{*edit} during re-denoising. This ensures that the velocity field during denoising accordingly tends to preserve these regions.

Effectiveness of MVG. Comparing Exp. ④ and ⑥, we observe that the introduction of MVG results in a decrease in structure similarity from 33.98 to 18.87, while PSNR increases from 21.97 dB to 24.99 dB, indicating a significant improvement in editing fidelity. As a trade-off for faithfulness to the original image, there is a decrease in CLIP similarity. Since MVG ensures that the overall structure of the edited image undergoes minimal changes, it imposes greater limitations on whole image editing, leading to a decrease in the whole image metric from 26.40 to 25.79 (-0.61). However, because MVG distinguishes between edited and non-edited regions and uses the evolving image to guide the editing of specific areas, the restriction on edited regions is greatly reduced, resulting in only a slight decrease of 0.36 in Edited CLIP similarity. This demonstrates that under the guidance of MVG, fidelity can be significantly enhanced while avoiding the constraints on edited regions that could lead to unchanged result.

5 Conclusion

We presented a novel RF-based method, namely DNAEdit, for text-guided image editing. By utilizing RF’s property of linear trajectory, we proposed a method to estimate accurate latents by calculating the velocity fields at specific timesteps through random sampling and linear interpolation. By analyzing the expected and predicted velocity fields, we presented DNA to align the image to the ideal noise directly in the Gaussian noise domain. We then introduced MVG to maintain background areas while guiding effective changes in editing regions. Theoretical analyses were provided to explain the effectiveness of DNA and MVG and their connections with existing RF-based editing methods. Experiments were conducted on the commonly used PIE-Bench and our newly improved long-text DNA-Bench. Both qualitative and quantitative results showed that our DNAEdit approach performed well on various editing tasks, producing high-quality edits faithful to the original image.

Limitations. As a training-free editing method, DNAEdit utilizes the strong priors of pre-trained T2I models by converting images into structured noise aligned with the given text. Therefore, it may fall short in achieving desired editing results for cases that lie outside the foundation T2I model’s prior.

Appendix

In this appendix, we provide the following materials:

- A More details of the DNA algorithms (referring to Sec. 3.2 in the main paper);
- B Theoretical analysis for rectified flow (RF)-based editing methods;
- C Detailed experimental setup, including more implementation details and the construction details of DNA-Bench (referring to Sec. 4.1 in the main paper);
- D More editing results of DNAEdit and more visual comparisons on both PIE-bench and DNA-bench (referring to Sec. 4.2 in the main paper);
- E Additional ablation studies on DNAEdit (referring to Sec. 4.3 in the main paper);
- F The results of applying DNAEdit to video editing;
- G Broader impacts.

A More Details of the DNA Algorithm

A.1 Detailed Derivation of the DNA Algorithm

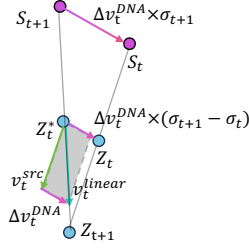


Figure 6: Direct noise alignment (DNA) for timestep t .

Assuming the noise is at S_{t+1} , the linear velocity v^{linear} at this point is given by $\frac{S_{t+1} - Z_{t+1}}{\sigma_{t+1}}$, while the velocity conditioned on source prompt v^{src} is represented by $v_\theta(Z_t^*, \psi^{src})$. To align the linear velocity with v_t^{src} , we move Z_t^* and S_{t+1} . Then Z_t can be derived by Eq. (11) using the velocity difference $\Delta v_t^{DNA} = \frac{Z_{t+1} - Z_t^*}{\sigma_{t+1} - \sigma_t} - v_t^{src}$:

$$Z_t = Z_t^* + \Delta v_t^{DNA}(\sigma_{t+1} - \sigma_t). \quad (11)$$

Accordingly, we need to shift the current Gaussian noise S_{t+1} to obtain a new Gaussian noise S_t to ensure that S_t , Z_t and Z_{t+1} still satisfy the properties of linear interpolation. Therefore, the ratio between S_t , Z_t and Z_{t+1} should adhere to the ratio specified in Eq. (12):

$$\begin{aligned} \frac{S_t - S_{t+1}}{Z_t - Z_t^*} &= \frac{\sigma_{t+1}}{\sigma_{t+1} - \sigma_t}, \\ S_t - S_{t+1} &= \frac{\sigma_{t+1}}{\sigma_{t+1} - \sigma_t} \times (Z_t - Z_t^*), \\ S_t - S_{t+1} &= \Delta v_t^{DNA} \times \sigma_{t+1}. \end{aligned} \quad (12)$$

Through straightforward derivation, we can obtain that the shift required to move S_{t+1} to S_t is $\Delta v_t^{DNA} \times \sigma_{t+1}$ at timestep t .

We provide additional visualizations in Fig. 7 to demonstrate the changes of noise S_t within the Gaussian noise space. Specifically, the noise difference $S_t - S_{t+3}$ is presented. It can be seen that as the DNA process progresses, the reference image's content is injected into the Gaussian noise through the difference in the velocity field.

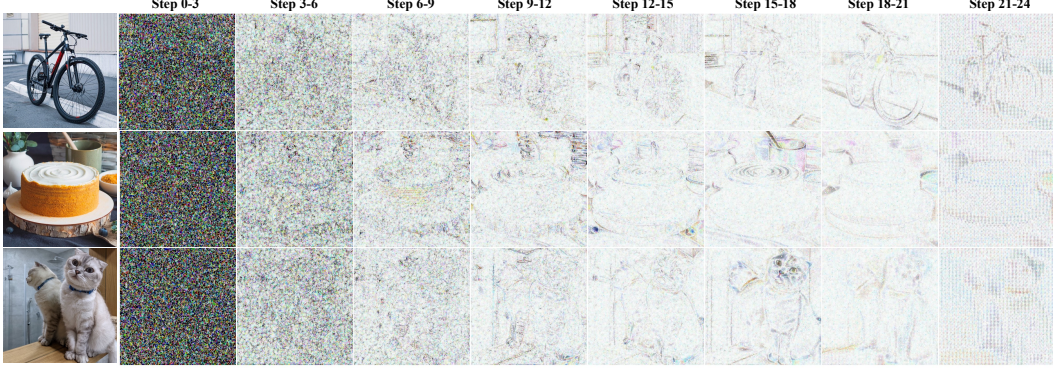
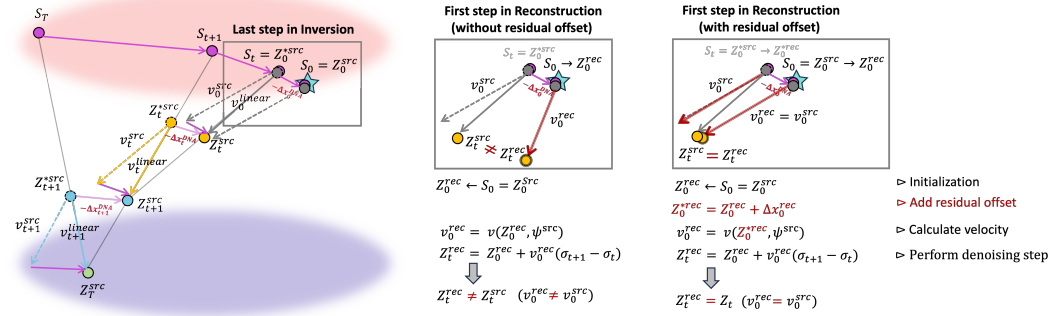


Figure 7: More visualization of the difference in Gaussian noise between S_t and S_{t+3} .



(a) DNAEdit inversion (left) and the first step of reconstruction (right)

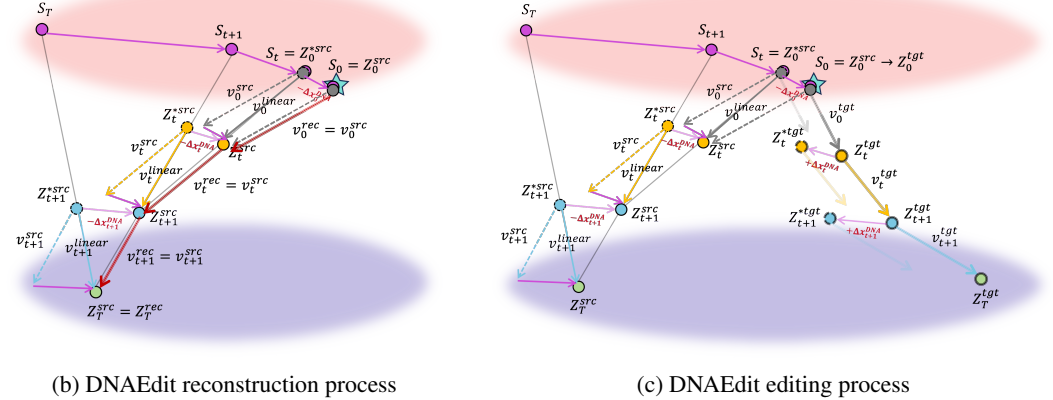


Figure 8: DNA reconstruction and editing without and with residual offset.

A.2 DNA Reconstruction without and with Residual Offset

Fig. 8a illustrates the inversion and reconstruction process, comparing the effect of adding the residual offset. The left side shows the standard inversion path (timesteps: $T \rightarrow t+1 \rightarrow t \rightarrow 0$), while the right side highlights the difference between reconstructions without and with the residual offset (for clarity, only the first step $t=0$ is visualized). Without the residual offset, the reconstructed latent Z_t^{rec} deviates due to the mismatched velocity directions between v_0^{rec} and v_0^{src} , leading to accumulated error. In contrast, reintroducing the residual offset aligns each timestep's velocity computation with the same noise latent used during inversion, which can be formulated as:

$$Z_t^{*rec} = Z_t^{rec} + \Delta x_t^{DNA} \Rightarrow Z_t^{*src}. \quad (13)$$

Algorithm 3 Reconstruction Process with Residual Offset

Input: Source image Z_T^{src} , Timesteps $\{\sigma_t\}_{t=0}^T$, RF v_θ , Source text ψ^{src} and target text ψ^{tgt}
Output: Reconstructed image Z_T^{tgt}
Inversion Init: Random Gaussian noise S_T
for $t = T - 1, \dots, 0$ **do**
 $Z_t^{src} \leftarrow Z_{t+1}^{src} \times \frac{\sigma_t}{\sigma_{t+1}} + S_{t+1} \times (1 - \frac{\sigma_t}{\sigma_{t+1}})$
 $v_t^{src} = v_\theta(Z_t^{src}, \psi^{src})$
 $v_t^{linear} = (Z_{t+1}^{src} - S_{t+1}) / \sigma_{t+1}$
 $\Delta v_t^{DNA} = v_t^{linear} - v_t^{src}$
 $S_t \leftarrow S_{t+1} + \Delta v_t^{DNA} \times \sigma_{t+1}$
 $Z_t^{src} \leftarrow Z_t^{src} + \Delta v_t^{DNA} \times (\sigma_{t+1} - \sigma_t)$
 $\Delta x_t^{DNA} = Z_t^{src} - Z_t^{src}$
end for
Reconstruction Init: $Z_0^{rec} \leftarrow S_0 = Z_0^{src}$
for $t = 0, \dots, T - 1$ **do**
 $Z_t^{rec} = Z_t^{rec} + \Delta x_t^{DNA} \Rightarrow Z_t^{*src}$ ▷ Add the residual offset back
 $v_t^{rec} = v_\theta(Z_t^{rec}, \psi^{src}) \Rightarrow v_\theta(Z_t^{*src}, \psi^{rec}) = v_t^{src}$ ▷ Calculate velocity v_t^{rec} using source text
 $Z_{t+1}^{rec} = Z_t^{rec} - v_t^{rec} \times (\sigma_{t+1} - \sigma_t) \Rightarrow Z_{t+1}^{src}$
end for
return $Z_T^{rec} \Rightarrow Z_T^{src}$

This corrected latent Z_t^{*rec} ensures that the velocity field can be computed consistently:

$$v_t^{rec} = v_\theta(Z_t^{*rec}, \psi^{src}) = v_\theta(Z_t^{*src}, \psi^{rec}) \Rightarrow v_t^{src} \quad (14)$$

As a result, the reconstruction can be formulated as:

$$Z_{t+1}^{rec} = Z_t^{rec} - v_t^{rec} \times (\sigma_{t+1} - \sigma_t) \Rightarrow Z_t^{rec} - v_t^{src} \times (\sigma_{t+1} - \sigma_t) = Z_{t+1}^{src}. \quad (15)$$

It becomes perfectly aligned with the original trajectory, eliminating cumulative errors and restoring the source latent precisely. This mechanism is essential for faithful and drift-free image recovery, and it is further illustrated in Fig. 8b and Algorithm 3.

A.3 DNA Editing with Residual Offset

Similarly, during the editing process (as illustrated in Fig. 8c and detailed in Algorithm 4), we incorporate the residual offset back into the latent representations at each timestep. Specifically, we adjust each latent Z_t^{tgt} by adding the pre-computed residual offset Δx_t^{DNA} , yielding a corrected latent Z_t^{*tgt} . This adjustment ensures that the velocity field v_t^{tgt} is computed using a latent aligned with the same noise used in the inversion process, thereby maintaining consistency between the inversion and editing trajectories. This alignment is crucial for preserving the structural integrity of the unedited regions. Without it, the mismatch between inversion and editing latents can lead to misaligned gradient directions, causing semantic drift and unintended changes to the background or identity of the source image. By correcting the editing trajectory with the residual offset, our method maintains a higher fidelity to the original content while allowing more precise and localized editing aligned with the target prompt.

B Theoretical Analysis between DNAEdit and FlowEdit

DNAEdit, as illustrated in Fig. 9b, can be viewed as a perfectly aligned, inversion-aware extension of FlowEdit (Fig. 9a). Unlike FlowEdit, which relies on independently sampled Gaussian noise at each timestep, DNAEdit assigns an optimal noise vector to each timestep via direct noise alignment. This alignment ensures the continuity of the target trajectory Z_t^{tgt} across timesteps and eliminates the accumulation of discretization errors that typically arise in FlowEdit.

The overview of FlowEdit is shown in Fig. 9a. It initializes $Z_T^{FE} = Z_T^{src}$. For each timestep t , Gaussian noise S_t is randomly sampled, and the source trajectory Z_t^{src} is interpolated between the

Algorithm 4 Editing Process with Residual Offset

Input: Source image Z_T , Timesteps $\{\sigma_t\}_{t=0}^T$, RF v_θ , Target text ψ^{tgt}

Output: Edited image Z_T^{tgt}

Inversion: See Algorithm 3

Editing Init: $Z_0^{tgt} \leftarrow S_0$

for $t = 0, 1, \dots, T-1$ **do**

$$Z_t^{*tgt} = Z_t^{tgt} + \Delta x_t^{\text{DNA}}$$

$$v_t^{tgt} = v_\theta(Z_t^{*tgt}, \psi^{tgt})$$

$$Z_{t+1}^{tgt} = Z_t^{tgt} - v_t^{tgt} \times (\sigma_{t+1} - \sigma_t)$$

end for

return Z_T^{tgt}

▷ Add the residual offset back

▷ Calculate velocity v_t^{tgt} using target text

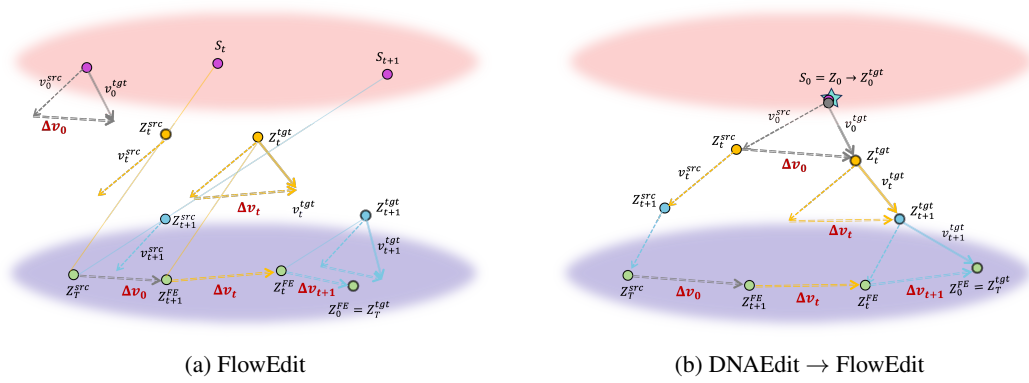


Figure 9: Illustration of the equivalence between FlowEdit and DNAEdit.

source image Z_T^{src} and the noise S_t . The target trajectory Z_t^{tgt} is derived using the parallelogram rule:

$$Z_t^{tgt} = Z_{t+1}^{\text{FE}} + Z_t^{src} - Z_T^{src}. \quad (16)$$

The velocity difference between the source and target is computed as: $\Delta v_t = v_\theta(Z_t^{tgt}, \psi^{tgt}) - v_\theta(Z_t^{src}, \psi^{src})$, and the editing trajectory from the source to target image is updated iteratively: $Z_t^{\text{FE}} = Z_{t+1}^{\text{FE}} + \Delta v_t \times (\sigma_{t+1} - \sigma_t)$.

In contrast, DNAEdit, as shown in Fig. 9b, also constructs a trajectory between the source and target images, but with key improvements. The algorithm initializes $Z_T^{\text{FE}} = Z_T^{src}$, and for each timestep t , the velocity difference is defined as: $\Delta v_t^{\text{DNA}} = v_\theta(Z_t^{*tgt}, \psi^{tgt}) - v_\theta(Z_t^{src}, \psi^{src})$ (Z_t^{src*} and Z_t^{tgt*} represent the latent variables Z_t^{src} and Z_t^{tgt} with residual offset, respectively; see Fig. 8c). The trajectory from the source to target images is then updated using: $Z_t^{\text{FE}} = Z_{t+1}^{\text{FE}} + \Delta v_t \times (\sigma_{t+1} - \sigma_t)$.

The most critical step is to prove that DNAEdit also satisfies the parallelogram rule (highlighted by the yellow parallelogram in Fig. 10b), as what is done in FlowEdit (yellow parallelogram in Fig. 10a), *i.e.*,

$$Z_t^{*tgt} = Z_{t+1}^{\text{FE}} + Z_t^{src*} - Z_T^{src}. \quad (17)$$

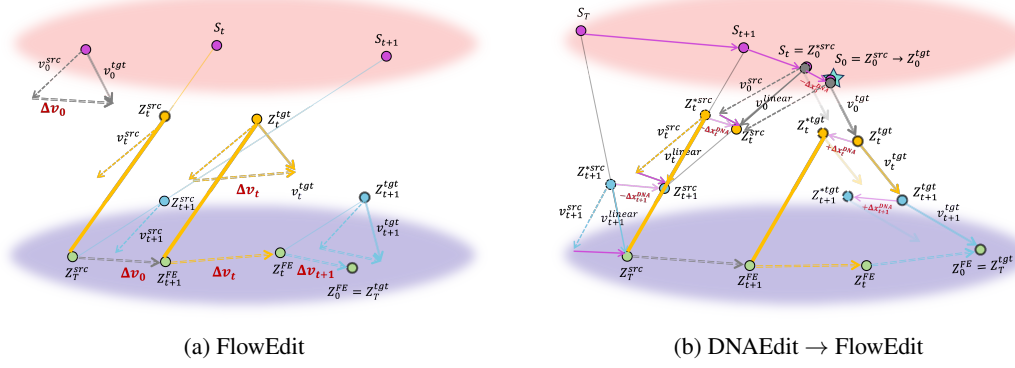


Figure 10: Parallelogram rule in FlowEdit and DNAEdit.

If this rule holds, the only difference between DNAEdit and FlowEdit lies in the selection of Gaussian noise at each timestep. The proof process is as follows:

$$\begin{aligned}
Z_t^{*tgt} &= Z_t^{tgt} + \Delta v_t^{\text{DNA}} \times (\sigma_{t+1} - \sigma_t) \\
&= Z_t^{tgt} + Z_t^{*src} - Z_t^{src} \\
&= Z_t^{tgt} + Z_t^{*src} - Z_T^{src} + Z_T^{src} - Z_t^{src} \\
&= Z_T^{src} + Z_t^{tgt} - Z_t^{src} + Z_t^{*src} - Z_T^{src} \\
&= Z_T^{src} + (Z_0^{tgt} + \sum_{i=0}^{t-1} Z_{i+1}^{tgt} - Z_i^{tgt}) - (Z_0^{src} + \sum_{i=0}^{t-1} Z_{i+1}^{src} - Z_i^{src}) + Z_t^{*src} - Z_T^{src} \\
&= Z_T^{src} + \sum_{i=0}^{t-1} (v_i^{tgt} - v_i^{src}) \times (\sigma_{i+1} - \sigma_i) + Z_t^{*src} - Z_T^{src} \\
&= Z_{t+1}^{\text{FE}} + Z_t^{*src} - Z_T^{src}
\end{aligned} \tag{18}$$

As shown in Fig. 10b, direct noise alignment ensures the relationship: $v_t^{src} \times (\sigma_{t+1} - \sigma_t) = Z_{t+1}^{src} - Z_t^{src}$. However, in FlowEdit, this relationship does not hold because Z_t^{src} and Z_{t+1}^{src} are generated by interpolating the source image with independently sampled noises. As a result, their difference does not necessarily equal the velocity vector, *i.e.*, $v_t^{src} \times (\sigma_{t+1} - \sigma_t) \neq Z_{t+1}^{src} - Z_t^{src}$. This inconsistency in FlowEdit is resolved by the direct noise alignment in DNAEdit, which ensures both the continuity and optimality of the trajectory.

Both DNAEdit and FlowEdit maintain a trajectory from the source to target image $\{Z_t^{\text{FE}}\}_{t=0}^T$. However, the primary difference lies in the continuity of the target trajectory $\{Z_t^{tgt}\}_{t=0}^T$. Specifically, in FlowEdit, the Gaussian noise for each timestep is independently sampled, which prevents the target trajectory from being continuous across adjacent timesteps. In contrast, DNAEdit aligns the noise from S_{t+1} to S_t , ensuring that the target trajectory is continuous across timesteps. This alignment enables DNAEdit to select an optimal noise sample, thereby eliminating discretization errors and producing a smoother trajectory.

C More Experiment Results

C.1 Implementation Details

In our experiments, we utilize the official implementations and default hyperparameters for those comparative methods [18, 23, 6, 2, 25, 7]. The exception is FTEdit [28], which is currently unavailable, and we use the results provided in its paper on the PIE-Bench. For our DNAEdit, the FLUX version is built upon the FLUX-dev [9] model, with the DNA steps set to 28, t_s set to 4 and CFG set to 2.5. In the SD version, we use the SD3.5-medium [21] model, with DNA steps set to 40, t_s set to 13, and CFG set to 3.5. Both versions have the MVG coefficient η set to 0.8 to balance background preservation and target editing. All experiments are conducted on an NVIDIA L40S GPU.





System: <div>  </div>		
Task: Please provide a more detailed description by combining the content of the image and the short prompt for the image-caption pairs I have provided to you, and simultaneously generate the corresponding editing prompts.		
Guidelines: <ul style="list-style-type: none"> - Please expand the description of the original image focusing on the target that needs editing, and simultaneously generate corresponding editing prompts. Both should be thorough yet concise, under 70 words. - Based on the provided editing instructions, generate new editing commands for the updated caption, requiring that they be as similar as possible in terms of grammar. - The new long editing prompt should only modify the parts in the original editing prompt that are different from the original short prompt. - Format your output as a strings without using the newline character. 		
Example: input: { original_prompt: "a [dog] is laying down on a white background", editing_prompt: "a [lion] is laying down on a white background" } output: { "new_long_prompt": "A dog with a fluffy coat and short legs is laying down on a pristine white background, showcasing its relaxed posture and soft fur.", "new_long_editing_prompt": "A lion with a fluffy coat and short legs is laying down on a pristine white background, showcasing its relaxed posture and soft fur." } 		
User: 	Original prompt: a yellow bird with a red beak sitting on a branch Editing prompt: a crochet bird with a red beak sitting on a branch	Response: New long prompt: A vibrant yellow bird with a striking red beak is perched gracefully on a slender branch, surrounded by lush green leaves and a textured tree trunk, creating a serene natural setting. New long editing prompt: A vibrant crochet bird with a striking red beak is perched gracefully on a slender branch, surrounded by lush green leaves and a textured tree trunk, creating a serene natural setting.
User: 	Original prompt: wolf howling at the moon with a outline of a wolf Editing prompt: wolf howling at the moon with a outline of a person	Response: New long prompt: A wolf is howling at the moon, silhouetted against a vibrant night sky filled with stars and surrounded by tall pine trees, all within the outline of a wolf's head. New long editing prompt: A wolf is howling at the moon, silhouetted against a vibrant night sky filled with stars and surrounded by tall pine trees, all within the outline of a person's head.
User: 	Original prompt: smoke Editing prompt: fire	Response: New long prompt: Thick plumes of smoke billow from the tall chimneys of an industrial plant, set against a backdrop of a clear blue sky with scattered clouds. The smoke rises high, creating a stark contrast with the surrounding environment, while a wind turbine stands nearby, highlighting the juxtaposition of industrial and renewable energy sources. New long editing prompt: Thick plumes of fire billow from the tall chimneys of an industrial plant, set against a backdrop of a clear blue sky with scattered clouds. The fire rises high, creating a stark contrast with the surrounding environment, while a wind turbine stands nearby, highlighting the juxtaposition of industrial and renewable energy sources.

Figure 11: Detailed prompt for constructing DNA-Bench and samples from DNA-Bench.

C.2 Details of DNA-Bench

We employ the advanced GPT-4o [22] to expand the short prompts in PIE-Bench into longer ones, creating our DNA-Bench. As illustrated in Fig. 11, we design prompts to achieve this expansion. Initially, reference images are input into GPT-4o to parse content and generate descriptions. To prevent hallucinations and ensure the description aligns with the editing intent, we provide the original short prompts, transforming the task into one that expands around these prompts. This method allows for a detailed description of the editing target while offering a comprehensive background description, enhancing alignment between image and text for improved background preservation and editing.

Our strategy effectively expands the original short prompts into longer ones. For example, in the 3rd row of Fig. 11, the original prompt was simply "smoke", which is too short to describe the editing target. In DNA-Bench, the image content is described in detail, aiding in preserving the original image's structure and non-editing areas during editing, while accurately modifying the editing target. We present experimental results and discussions on training-free editing using long texts in both the main text and Fig. 16 in this appendix. Although long texts may pose some inconvenience to humans, the progress made by modern MLLMs allows us to easily integrate them into real-world applications to help expand the initial prompts provided by users into longer prompts that are more conducive to editing. Thus, we believe that DNA-Bench, with its high-quality long text prompts, is important for the future development and evaluation of text-guided editing methods.

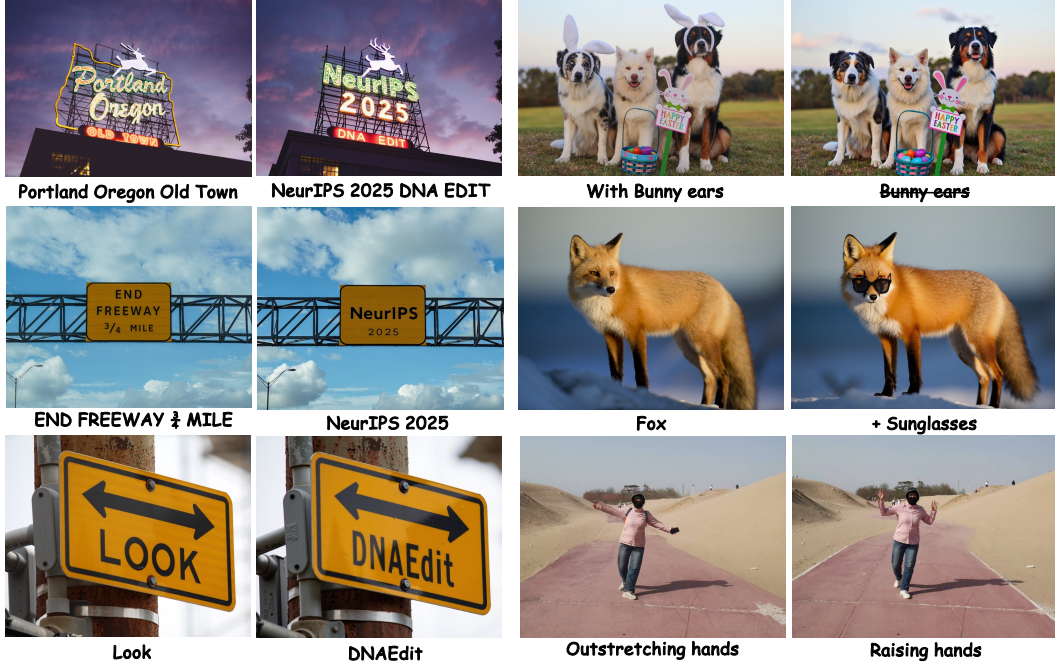


Figure 12: More results of DNAEdit on real images. Original(Left) vs. Edited(Right).

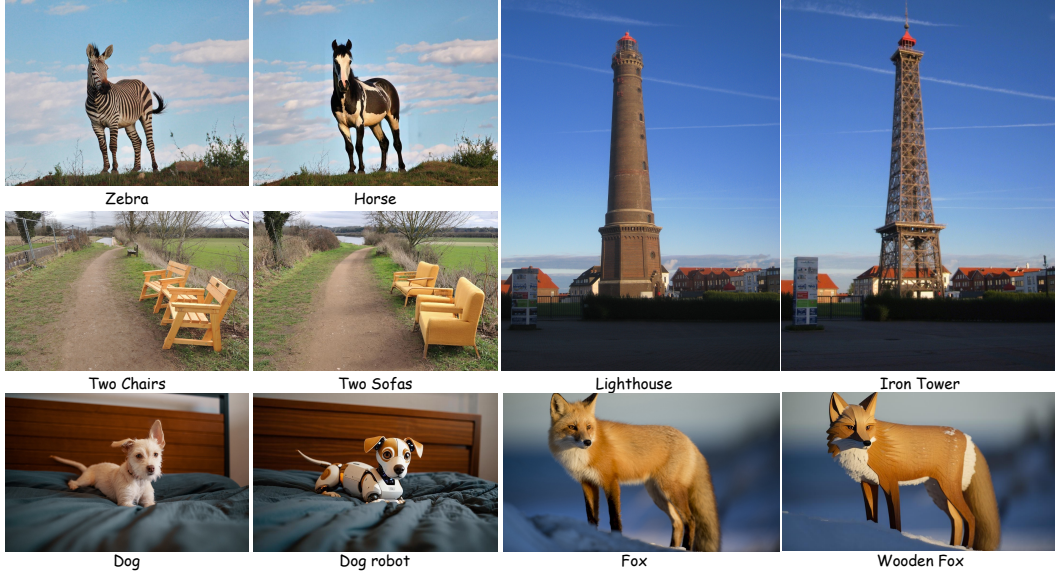


Figure 13: More results of DNAEdit on real images. Original(Left) vs. Edited(Right).

D More Visual Comparisons

D.1 More Visual Results of DNAEdit

In Fig. 12 and Fig. 13, we showcase additional results of DNAEdit applied to high-resolution real-world images. In each image pair, the original is on the left, and the edited result is on the right. DNAEdit demonstrates high-quality editing capabilities on these images. For example, in the first column of Fig. 12, DNAEdit achieves precise text editing, thanks to the powerful text generation capabilities of the T2I model FLUX, while preserving other areas of the image. The second column highlights DNAEdit’s effectiveness in tasks such as addition and deletion. Additionally, in the 3rd

row of the right column, DNAEdit successfully changes a human pose from "outstretching hands" to "raising hands," illustrating its capability in non-rigid editing tasks. In Fig. 13, we present more object-level editing results, including changes in object type and material. For instance, in the 2nd column, a lighthouse is transformed into an iron tower, with details like line-shaped clouds in the sky perfectly preserved. The last row demonstrates the effect of changing an object's material, where the original material is completely altered, yet the object's original features, such as posture, are retained.

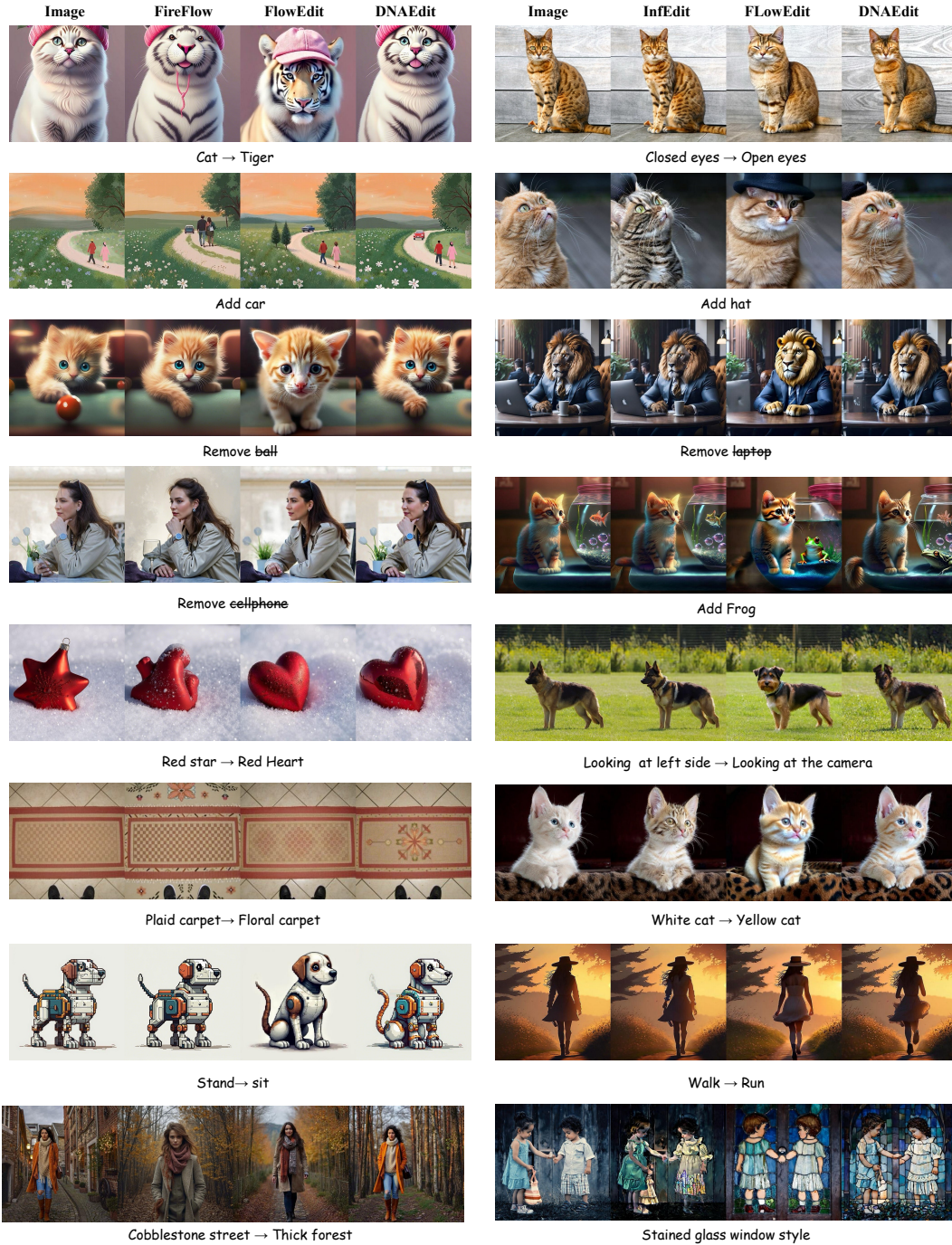


Figure 14: More visual comparisons on PIE-Bench. Left: FLUX-based, Right: SD-based.

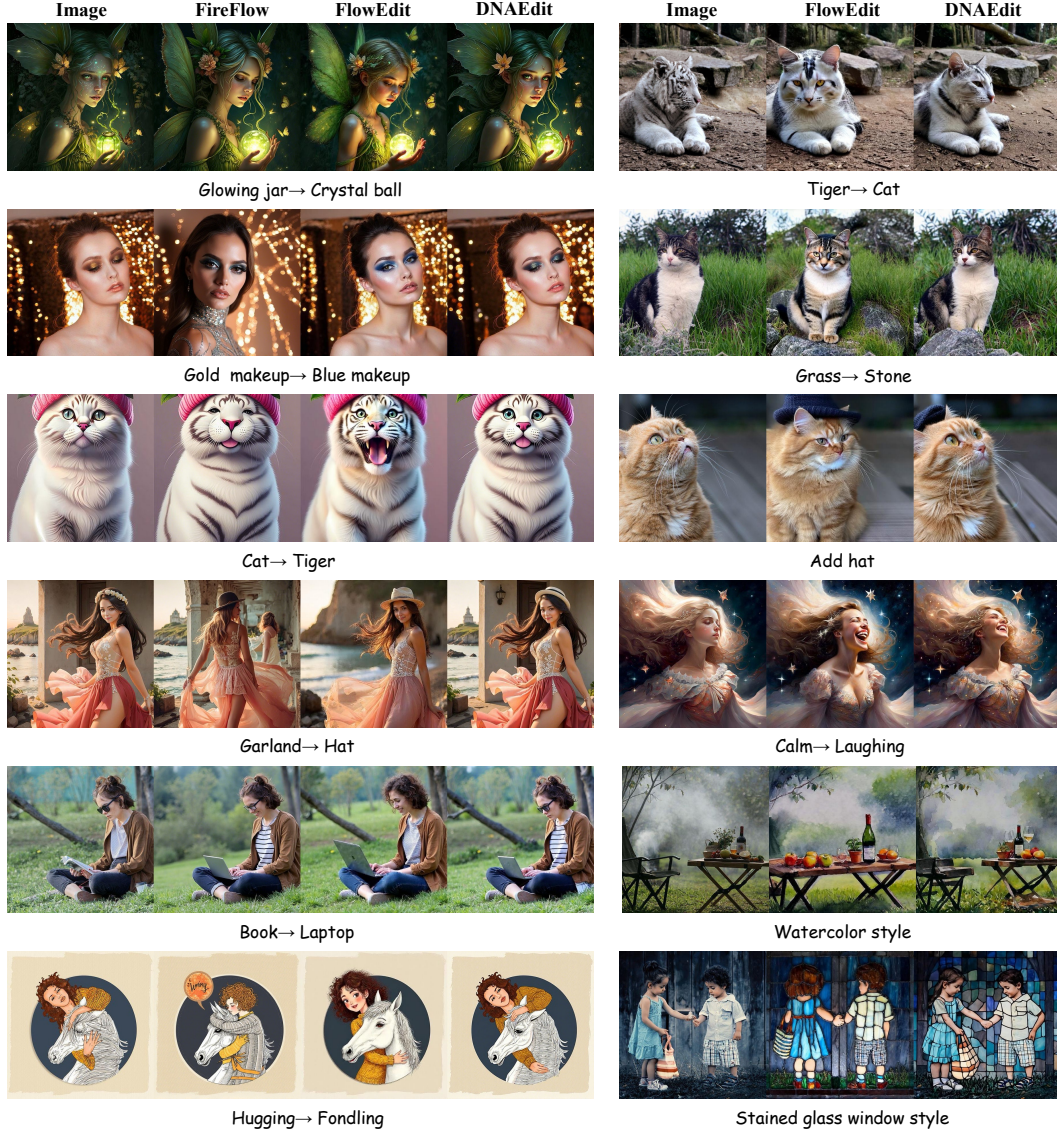


Figure 15: More visual comparisons on DNA-Bench. Left: FLUX-based, Right: SD-based.

D.2 Comparisons on PIE-Bench

We present additional visual comparisons in Fig. 14, where the left side shows results from methods based on the FLUX model, and the right side displays results from methods based on the SD series. Our approach consistently outperforms other methods across various editing tasks. For instance, in the non-rigid editing task on the left side, row 7, FireFlow fails to make the dog sit, while FlowEdit succeeds but significantly alters the dog’s appearance. In contrast, our method preserves the dog’s original features while successfully changing its posture from standing to sitting. Additionally, as can be seen in row 8 on the left side, our method effectively tackles the challenging task of changing large backgrounds, maintaining the woman’s appearance almost unchanged while transforming the background from a street to a forest. Methods based on SD also achieve similar results. On the right side, row 8, our method successfully stylizes the entire image while preserving the characteristics of the original elements, such as the child’s actions and attire, aligning more closely with our intent.

D.3 Comparisons on DNA-Bench

In Fig. 15, we additionally present comparative results under long text descriptions from the DNA-Bench. With the introduction of long text, RF-based editing methods show some improvements, such as more accurate backgrounds. However, our method still maintains advantages. For example, in the 4th row on the left, FireFlow alters the entire image structure. Although FlowEdit appears to preserve the structure, a comparison with our method reveals that both the person and the background undergo significant changes. Similarly, in the 5th row, our method better preserves the background (such as the tree trunk) and the sunglasses on the person’s face, while successfully changing the book into a laptop.



Figure 16: Visual comparison between results from PIE-Bench and DNA-Bench.

E More Ablation Studies

E.1 Ablation on Effect of Long-text Prompt in DNA-Bench

In Fig. 16, we present a comparison of various methods on PIE-Bench and DNA-Bench to demonstrate the impact of long text on image editing. As discussed in Sec 4.2 of main paper, a longer source prompt can provide a more detailed description of the image, resulting in noise that is more aligned with the source prompt. During editing, since the target prompt is similar to the source prompt, the non-edit regions remain unchanged. For example, in the 1st row, 3rd column of Fig. 16, under a long text prompt, the description "cobblestone path" leads to noticeable changes in the ground in FireFlow’s editing results, making it more consistent with the original image. Our DNAEdit method also benefits from this; under a short text prompt, the paw area transforms into a larger flower, whereas under a long text prompt, both the paw and flower are more consistent with the original image. This effect is even more pronounced in the third row, where both FireFlow and DNAEdit show significant changes in the image background under short text prompts. However, under long text prompts, thanks to the detailed background description, the edited results better match the original scene. In addition, long text prompts enable for more precise editing targets. In the second row, the editing goal is to replace the woman with a storm-trooper. Under the limited expression of a short text prompt, the model mistakenly applies the edit to the shirt’s pattern. With a long text prompt, which provides more accurate alignment between the scene and text, the edit is successfully applied to the woman. Combined with the results shown in the main paper, we can see that long text prompts in DNA-Bench offer significant benefits for the most recent RF-based editing models.

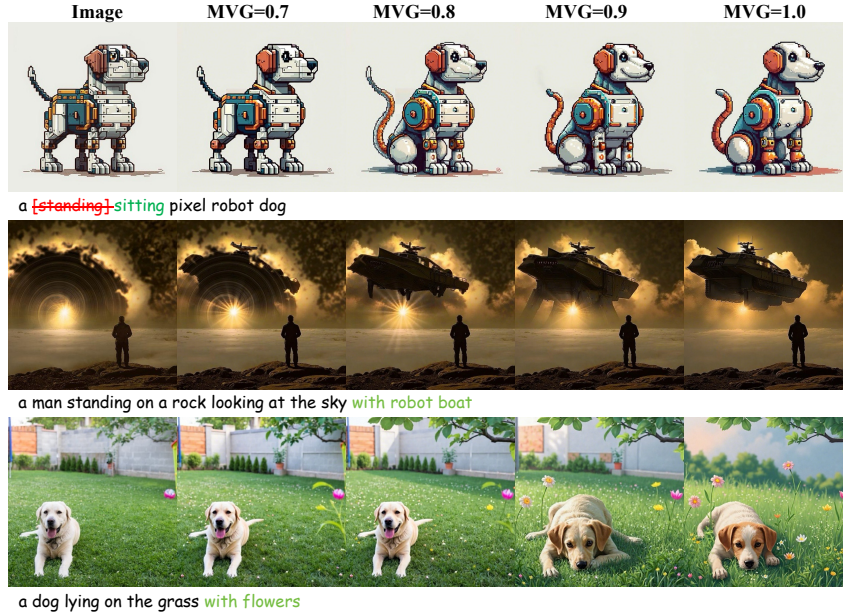


Figure 17: Comparison between different MVG coefficients η .

E.2 Ablation on Effect of MVG Coefficient η

In Fig. 17, we demonstrate the impact of different MVG coefficients on editing results. Fig. 17 clearly shows that MVG can effectively ensure the faithfulness to the reference image. For instance, in the third row, when the MVG is set to 1.0, the overall layout of the image changes significantly. As the MVG decreases, the structure becomes more similar to the original image, with flowers added to the grass while maintaining structural consistency at MVG values of 0.8 and 0.7. However, an excessively large MVG can lead to editing failures. For example, in the 1st row, with an MVG of 0.7, the dog is not edited to sit, whereas results with MVG greater than 0.8 successfully achieve this. Moreover, compared to MVG values of 0.9 and 1.0, the result at 0.8 more closely resembles the original appearance of the dog, aligning with our editing intent. This experiment demonstrates that

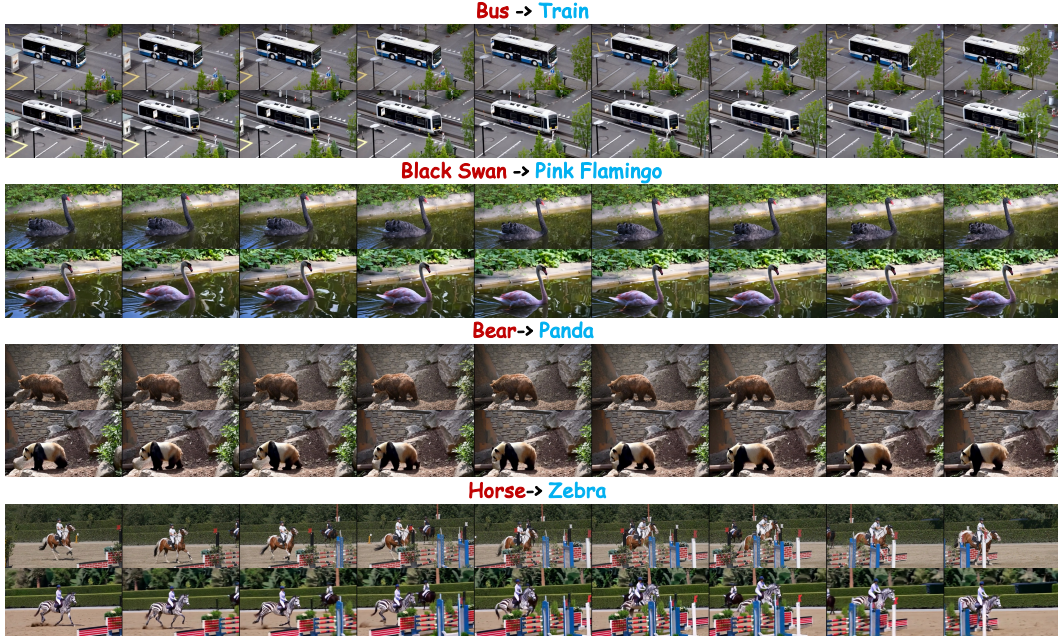


Figure 18: Visual results of DNAEdit for video editing task.

an appropriate MVG can effectively preserve non-editing areas without affecting them. Additionally, by adjusting the MVG, users can control the intensity of the edits according to their needs, achieving more flexible editing results.

F DNAEdit for Video Editing

In Fig. 18, we present the results of DNAEdit applied to more challenging videos editing task [10]. We conduct experiments using the Rectified Flow-based text-to-video (T2V) model, Wan2.1 [24]. Since DNAEdit is a model-agnostic algorithm, we achieve impressive editing effects **without any modifications to the model**. As illustrated, DNAEdit accurately transforms the target, such as changing a bear into a panda, while preserving the original structure and time consistency. This demonstrates DNAEdit’s strong potential for application in various existing and future flow-based generative models, enabling more valuable applications.

G Broader Impacts

Our proposed image editing method has several potential societal impacts, both positive and negative. On the positive side, this method can enhance creative industries by providing artists and designers with powerful tools for content creation and modification. However, there are potential negative impacts to consider. The technology could be misused for creating misleading or harmful content, which could have significant implications for privacy and security. To mitigate these risks, we suggest implementing mechanisms for monitoring and controlling the use of the technology, such as gated releases, and developing tools to detect and counteract malicious uses.

References

- [1] Mingdeng Cao, Xintao Wang, Zhongang Qi, Ying Shan, Xiaohu Qie, and Yinqiang Zheng. Masactrl: Tuning-free mutual self-attention control for consistent image synthesis and editing. In *Proceedings of the IEEE/CVF International Conference on Computer Vision*, pages 22560–22570, 2023.
- [2] Yingying Deng, Xiangyu He, Changwang Mei, Peisong Wang, and Fan Tang. Fireflow: Fast inversion of rectified flow for image semantic editing. *arXiv preprint arXiv:2412.07517*, 2024.

- [3] Patrick Esser, Sumith Kulal, Andreas Blattmann, Rahim Entezari, Jonas Müller, Harry Saini, Yam Levi, Dominik Lorenz, Axel Sauer, Frederic Boesel, et al. Scaling rectified flow transformers for high-resolution image synthesis. In *Forty-first International Conference on Machine Learning*, 2024.
- [4] Ayaan Haque, Matthew Tancik, Alexei A Efros, Aleksander Holynski, and Angjoo Kanazawa. Instruct-nerf2nerf: Editing 3d scenes with instructions. In *Proceedings of the IEEE/CVF International Conference on Computer Vision*, pages 19740–19750, 2023.
- [5] Amir Hertz, Ron Mokady, Jay Tenenbaum, Kfir Aberman, Yael Pritch, and Daniel Cohen-or. Prompt-to-prompt image editing with cross-attention control. In *The Eleventh International Conference on Learning Representations*, 2023.
- [6] Xuan Ju, Ailing Zeng, Yuxuan Bian, Shaoteng Liu, and Qiang Xu. Direct inversion: Boosting diffusion-based editing with 3 lines of code. *arXiv preprint arXiv:2310.01506*, 2023.
- [7] Vladimir Kulikov, Matan Kleiner, Inbar Huberman-Spiegelglas, and Tomer Michaeli. Flowedit: Inversion-free text-based editing using pre-trained flow models. *arXiv preprint arXiv:2412.08629*, 2024.
- [8] Black Forest Labs. Flux. <https://github.com/black-forest-labs/flux>, 2024. Accessed: 2024-11-14.
- [9] Black Forest Labs. Official weights of FLUX.1 dev. <https://huggingface.co/black-forest-labs/FLUX.1-dev>, 2024. Accessed: 2024-11-14.
- [10] Minghan Li, Chenxi Xie, Yichen Wu, Lei Zhang, and Mengyu Wang. Five: A fine-grained video editing benchmark for evaluating emerging diffusion and rectified flow models. *arXiv preprint arXiv:2503.13684*, 2025.
- [11] Shanglin Li, Bohan Zeng, Yutang Feng, Sicheng Gao, Xiuhui Liu, Jiaming Liu, Lin Li, Xu Tang, Yao Hu, Jianzhuang Liu, et al. Zone: Zero-shot instruction-guided local editing. In *Proceedings of the IEEE/CVF Conference on Computer Vision and Pattern Recognition*, pages 6254–6263, 2024.
- [12] Yaron Lipman, Ricky T. Q. Chen, Heli Ben-Hamu, Maximilian Nickel, and Matthew Le. Flow matching for generative modeling. In *The Eleventh International Conference on Learning Representations*, 2023.
- [13] Xingchao Liu, Chengyue Gong, and qiang liu. Flow straight and fast: Learning to generate and transfer data with rectified flow. In *The Eleventh International Conference on Learning Representations*, 2023.
- [14] Yongjia Ma, Donglin Di, Xuan Liu, Xiaokai Chen, Lei Fan, Wei Chen, and Tonghua Su. Adams bashforth moulton solver for inversion and editing in rectified flow. *arXiv preprint arXiv:2503.16522*, 2025.
- [15] Daiki Miyake, Akihiro Iohara, Yu Saito, and Toshiyuki Tanaka. Negative-prompt inversion: Fast image inversion for editing with text-guided diffusion models. *arXiv preprint arXiv:2305.16807*, 2023.
- [16] Ron Mokady, Amir Hertz, Kfir Aberman, Yael Pritch, and Daniel Cohen-Or. Null-text inversion for editing real images using guided diffusion models. In *Proceedings of the IEEE/CVF Conference on Computer Vision and Pattern Recognition*, pages 6038–6047, 2023.
- [17] Gaurav Parmar, Krishna Kumar Singh, Richard Zhang, Yijun Li, Jingwan Lu, and Jun-Yan Zhu. Zero-shot image-to-image translation. In *ACM SIGGRAPH 2023 Conference Proceedings*, pages 1–11, 2023.
- [18] Litu Rout, Yujia Chen, Nataniel Ruiz, Constantine Caramanis, Sanjay Shakkottai, and Wen-Sheng Chu. Semantic image inversion and editing using rectified stochastic differential equations. *arXiv preprint arXiv:2410.10792*, 2024.
- [19] Jiaming Song, Chenlin Meng, and Stefano Ermon. Denoising diffusion implicit models. In *International Conference on Learning Representations*, 2021.
- [20] StabilityAI. Official weights of SD3 medium diffusers. <https://huggingface.co/stabilityai/stable-diffusion-3-medium-diffusers>, 2024. Accessed: 2024-11-14.
- [21] StabilityAI. Official weights of SD3.5 medium. <https://huggingface.co/stabilityai/stable-diffusion-3.5-medium>, 2024. Accessed: 2024-11-14.
- [22] OpenAI Team. Gpt-4o system card, 2024.
- [23] Narek Tumanyan, Michal Geyer, Shai Bagon, and Tali Dekel. Plug-and-play diffusion features for text-driven image-to-image translation. In *Proceedings of the IEEE/CVF Conference on Computer Vision and Pattern Recognition*, pages 1921–1930, 2023.

- [24] Team Wan. Wan: Open and advanced large-scale video generative models. *arXiv preprint arXiv:2503.20314*, 2025.
- [25] Jiangshan Wang, Junfu Pu, Zhongang Qi, Jiayi Guo, Yue Ma, Nisha Huang, Yuxin Chen, Xiu Li, and Ying Shan. Taming rectified flow for inversion and editing. *arXiv preprint arXiv:2411.04746*, 2024.
- [26] Z. Wang, A.C. Bovik, H.R. Sheikh, and E.P. Simoncelli. Image quality assessment: From error visibility to structural similarity. *IEEE Transactions on Image Processing*, page 600–612, 2004.
- [27] Chengdong Wu, Ling-Qiao Huang, Qianxi Zhang, Binyang Li, Lei Ji, Fan Yang, Guillermo Sapiro, and Nan Duan. Godiva: Generating open-domain videos from natural descriptions. 2021.
- [28] Pengcheng Xu, Boyuan Jiang, Xiaobin Hu, Donghao Luo, Qingdong He, Jiangning Zhang, Chengjie Wang, Yunsheng Wu, Charles Ling, and Boyu Wang. Unveil inversion and invariance in flow transformer for versatile image editing. *arXiv preprint arXiv:2411.15843*, 2024.
- [29] Sihan Xu, Yidong Huang, Jiayi Pan, Ziqiao Ma, and Joyce Chai. Inversion-free image editing with language-guided diffusion models. In *Proceedings of the IEEE/CVF Conference on Computer Vision and Pattern Recognition*, pages 9452–9461, 2024.
- [30] Zexuan Yan, Yue Ma, Chang Zou, Wenteng Chen, Qifeng Chen, and Linfeng Zhang. Eedit: Rethinking the spatial and temporal redundancy for efficient image editing. *arXiv preprint arXiv:2503.10270*, 2025.
- [31] Zhen Yang, Ganggui Ding, Wen Wang, Hao Chen, Bohan Zhuang, and Chunhua Shen. Object-aware inversion and reassembly for image editing. *arXiv preprint arXiv:2310.12149*, 2023.
- [32] Richard Zhang, Phillip Isola, Alexei A. Efros, Eli Shechtman, and Oliver Wang. The unreasonable effectiveness of deep features as a perceptual metric. In *2018 IEEE/CVF Conference on Computer Vision and Pattern Recognition*, 2018.
- [33] Tianrui Zhu, Shiyi Zhang, Jiawei Shao, and Yansong Tang. Kv-edit: Training-free image editing for precise background preservation. *arXiv preprint arXiv:2502.17363*, 2025.